PAPER

Energetically favoured defects in dense packings of particles on spherical surfaces†

Stefan Paquay,*[a] Halim Kusumaatmaja,[b] David J. Wales,[c] Roya Zandi[d] and Paul van der Schoot[ae]

The dense packing of interacting particles on spheres has proved to be a useful model for virus capsids and colloidosomes. Indeed, icosahedral symmetry observed in virus capsids corresponds to potential energy minima that occur for magic numbers of, *e.g.*, 12, 32 and 72 identical Lennard-Jones particles, for which the packing has exactly the minimum number of twelve five-fold defects. It is unclear, however, how stable these structures are against thermal agitation. We investigate this property by means of basin-hopping global optimisation and Langevin dynamics for particle numbers between ten and one hundred. An important measure is the number and type of point defects, that is, particles that do not have six nearest neighbours. We find that small icosahedral structures are the most robust against thermal fluctuations, exhibiting fewer excess defects and rearrangements for a wide temperature range. Furthermore, we provide evidence that excess defects appearing at low non-zero temperatures lower the potential energy at the expense of entropy. At higher temperatures defects are, as expected, thermally excited and thus entropically stabilised. If we replace the Lennard-Jones potential by a very short-ranged (Morse) potential, which is arguably more appropriate for colloids and virus capsid proteins, we find that the same particle numbers give a minimum in the potential energy, although for larger particle numbers these minima correspond to different packings. Furthermore, defects are more difficult to excite thermally for the short-ranged potential, suggesting that the short-ranged interaction further stabilises equilibrium structures.

1 Introduction

Virus capsids[1] and colloidosomes[2] have been successfully modelled as dense packings of spherical particles constrained to a spherical surface, in particle-based[3–5] and phase-field calculations.[6] The equilibrium packings follow from the interplay between the curvature of the sphere and the interaction between the particles. For fixed particle size and surface coverage, increasing the radius of curvature of the surface leads to packings that exhibit varying numbers of isolated point defects that, for large enough particle numbers, condense into clusters of defects.[6–11] Here, defects are particles that do not have the ideal six-fold coordination. Studies of particles on unduloids and catenoids have shown that for small particle numbers a Lennard-Jones potential produces different minimum energy structures compared to a purely repulsive Coulomb potential, showing that the range

and type of interaction also affect the geometry of particle packings on curved surfaces.[12] For packings on spherical surfaces, the minimum energy structures for $N = 12$, 24, 32, 44 and 48 particles are the same for the Lennard-Jones and repulsive Coulomb potential, whereas for many other sizes, including 72, these are different.[13,14]

In their study of why spherical viruses almost invariably exhibit icosahedral symmetry, Zandi *et al.*[4] found by Monte Carlo simulation of Lennard-Jones particles on a spherical surface that, if the particle number allows it, the equilibrium packings do in fact have icosahedral symmetry. This effect occurs for the magic numbers $N = 12$, 32 and 72, corresponding to $T = 1$, 3 and 7 icosahedral symmetry. By allowing a switch between larger and smaller particle sizes, modeling pentameric and hexameric capsomeres, icosahedral symmetry is also recovered for $N = 42$, which is the $T = 4$ structure. Fejer *et al.* studied a different model of rigid bodies consisting of an attractive disk and two repulsive Lennard-Jones axial sites on top and bottom. These sites induce a preferred curvature. In this model, icosahedral packings turn out to be local potential energy minima for $N = 12$, 32 and 72, but the $T = 4$ icosahedral zero temperature structure for $N = 42$ is only a minimum energy structure if the disks assemble on top of a template.[15] In the single-particle description that we follow, all other particle numbers give non-icosahedral structures, often

[a] *Department of Applied Physics, Technische Universiteit, Eindhoven, The Netherlands. E-mail: s.paquay@tue.nl*
[b] *Department of Physics, University of Durham, UK*
[c] *Department of Chemistry, University of Cambridge, UK*
[d] *Department of Physics and Astronomy, University of California, Riverside, USA*
[e] *Instituut voor Theoretische Fysica, Universiteit Utrecht, The Netherlands*
† Electronic supplementary information (ESI) available. See DOI: 10.1039/c6sm00489j

with more than the minimum required twelve five-fold point defects.

Apparently, even for a single particle size, the icosahedrally packed structures have a lower potential energy per particle than the packings of adjacent sizes, at least for the low non-zero temperatures considered.[4] This result suggests that viruses prefer icosahedral symmetry simply because it is the most optimal packing for the effective interaction between the capsomeres. The Monte Carlo simulations of ref. 4 are consistent with the zero-temperature simulated annealing studies of Lennard-Jones particles packings by Voogd,[13] in the sense that they recover potential energy minima at the same sizes. However, the latter study provides more detail about the symmetry of all the packings found. Interestingly, Voogd identifies the global minimum for the $N = 72$ packing with a D_{5h} point group, rather than an icosahedral one, which is one of the structures that Zandi *et al.* identified at this size. This discrepancy could be due to the non-zero temperature in the simulations of Zandi *et al.*, hinting at the potential importance of entropy. Indeed, our calculations of the potential energy for both packings confirm that the D_{5h} packing has lower potential energy while counterintuitively, the icosahedral packing with fewer defects is entropically stabilised at a non-zero temperature. A similar finding is reported by Altschuler *et al.* for the Thomson problem for $N = 42$.[16]

This analysis suggests that temperature could play an important role in the thermodynamic stability of the symmetry of dense packings of particles on a spherical surface. For non-zero temperature, minimum energy does not imply minimum free energy. Indeed, our computer "experiments" reveal that for certain numbers of Lennard-Jones particles confined to a spherical surface, energy favours excess defects, *i.e.*, these packings have more than twelve defects for very low temperatures. Such energetically stabilised defects also appear for the Thomson problem[14,17] and as grain boundary scars.[6–11] Of course, at higher temperatures, entropy favours excess defects, in the form of thermally excited dislocations and/or disclinations analogous to melting in a 2D flat surface. For an extensive discussion we refer to the review of Strandburg.[18]

Another question that arises is how representative the atomic Lennard-Jones potential is for interactions between complex particles such as proteins and colloids, and how sensitive the structure of dense particle packings on curved templates is to the shape of the potential. This question is relevant because interactions between proteins are arguably better described by a short-ranged potential,[19–21] and Van der Waals interactions between colloids are also shorter-ranged (stickier) than predicted by the Lennard-Jones model.[22] For example, the colloidosomes of the Manoharan group are induced by the presence of polymer molecules that give rise to extremely short-ranged depletion interactions between the colloids.[23] For three-dimensional clusters it is already known that the range of the potential strongly influences the potential energy landscape. Previous work has shown that the shorter ranged the attractive part of the potential, the larger the number of local energy minima for a given number of particles.[24] Furthermore, for small clusters of short-ranged particles it was found that

temperature has a significant influence on the relative stability of different packings.[25] Finally, in a recent study of particles on ellipsoidal surfaces, Burke *et al.* found that the potential softness plays a crucial role in determining the particle number at which defects begin to appear.[26]

To address this issue in the context of particles confined to spherical surfaces, we consider a Morse potential of much shorter range than the Lennard-Jones form. For $N = 32$ and $N \leq 24$, we find for the same particle numbers deep local potential energy minima that also turn out to have the same structure. For larger N, the Morse potential produces deeper local minima in the potential energy landscape as a function of the N. Furthermore, for those sizes that are a local minimum in the potential energy for both the Morse and Lennard-Jones potential, the particle arrangement proved different. Hence, for a shorter-ranged potential, for the same N, different packings minimise the potential energy. For Morse particles it also proved more difficult to thermally excite defects, indicating that a shorter-ranged potential stabilises the structures. This property is especially clear in the case of the $T = 3$ icosahedron for $N = 32$.

However, we find that the $T = 7$ icosahedron for $N = 72$ is no longer an equilibrium packing, nor a potential energy minimum. Thus, while the range of the interaction potential broadens the temperature range over which structures are stable, it also influences the symmetry of the equilibrium packing itself. A similar observation was reported for simulations of disks with an adhesive edge confined to a spherical surface.[3] For adhesive disks, the effective range of attraction is zero, and in this case, the global minima for both $N = 32$ and $N = 72$ are no longer icosahedral packings. Thus, although a shorter range appears to help stabilise the equilibrium structures over a larger temperature range, it also changes the symmetry of the preferred packing.

Because in our simulations the particles fluctuate between different packings, we can obtain free energy differences simply by determining the probability of finding each packing. From this probability we determine that the icosahedral packing, which has the fewest defects, is indeed entropically more favourable than the D_{5h} structure, confirming that the ground state can exhibit excess defects. This is similar to experimental observations and computational results for very much larger systems in the form of grain boundary scars[6,10] and for packings of electrons on a sphere (the Thomson problem).[14,17] Grain boundary scars are predicted to appear around $N \geq 360$[10] based on elasticity theory, while excess defects in the form of scars and rosettes appear for $N \geq 410$ in the Thomson problem.[8,17] On ellipsoidal surfaces Burke *et al.* found that for hard particles, excess defects are stable for systems from $N \geq 200$.[26] In this study we consider significantly smaller particle numbers $10 \leq N \leq 100$. We note that in ref. 14 some minimum energy structures with excess defects for N as low as 44 have been identified, albeit that they do not form scars.

The remainder of this paper is organised as follows. First we describe in Section 2 the computational methods. We also provide a discussion of how we quantify defects and how we characterise them. Then, in Section 3, we discuss how temperature

influences the stability of packings of Lennard-Jones particles. In Section 4 we discuss the appearance of defects in the global minimum and determine free energy differences between the packings based on how often they are encountered. We continue in Section 5 to show that the equilibrium structures of Morse particles are much more robust against thermal fluctuations than those of Lennard-Jones particles, but that the minimum energy packings tend to differ from the Lennard-Jones packings at larger N. Finally, in Section 6, we underline the most important implications of the three different aspects of this work discussed above.

2 Methods

We consider packings of two different types of particle on a spherical surface. The first model employs the well-known Lennard-Jones potential, allowing us to directly compare our results with those of Zandi et al.[4] and Voogd.[13] We write the Lennard-Jones potential in terms of the equilibrium spacing, r_0, rather than the more usual zero-potential distance, to allow for a straightforward comparison with the Morse potential later on. Specifically, we have

$$V_{LJ}(r) = \varepsilon \left[\left(\frac{r_0}{r} \right)^{12} - 2 \left(\frac{r_0}{r} \right)^6 \right]. \qquad (1)$$

The minimum value $-\varepsilon$ occurs at $r = r_0$, so ε can be treated as the interaction strength or pair well depth. The second model employs the Morse potential

$$V_M(r) = \varepsilon \left[e^{-2\alpha(r-r_0)} - 2e^{-\alpha(r-r_0)} \right]. \qquad (2)$$

In eqn (2), the parameters ε and r_0 have the same meaning as in eqn (1), but now there is an additional parameter α, which can be used to tune the interaction range. In this work we set α to a specific value to model the interaction potential induced by depletants that the Manoharan group propose to discuss their experiments on colloidosomes.[23] We do this by fixing the ratio of the distances at which the potential exhibits a minimum and where it is only one tenth of that well depth. Applying this procedure leads to a value for the range parameter of $\alpha = (61.2 \pm 2)/r_0$, which for convenience we rounded to $\alpha = 60/r_0$. Such a large value for α leads to a much faster decay in the interaction strength and destabilises the liquid phase.[23,27–29] We specifically choose one tenth of the well depth because the separation from the minimum covers most of the peak shape, and hence we expect to obtain a better match. We performed calculations for $\alpha = 72$ as well and found qualitatively similar results. In particular, for $N = 72$ we find the same minimum energy structures in the same order, albeit at slightly different (higher) total potential energies.

In our Langevin dynamics simulations, performed with the LAMMPS program,[30] we truncate and shift the potential at some cutoff distance r_c by defining as actual interaction potential $V(r) = V_{LJ/M}(r) - V_{LJ/M}(r_c)$, where the subscript LJ denotes the Lennard-Jones potential and subscript M the Morse potential. We take as time unit the Langevin damping time τ_L, which describes the time over which the velocity autocorrelation decays. For our purposes, the exact value of the damping time should be irrelevant because all our simulations focus on systems under conditions of thermodynamic equilibrium. We take $r_c = 2.5r_0/2^{1/6} \approx 2.2272r_0$, at which the untruncated Lennard-Jones and Morse potentials have values of -0.016ε and $-2.1 \times 10^{-32} \approx 0\varepsilon$ respectively. The distance r_c corresponds to a cut-off at exactly 2.5σ in terms of the more common Lennard-Jones distance parameter σ. Furthermore, ε will serve as the reference energy unit and r_0 as reference length unit, producing a reference mass unit of $m_0 = \varepsilon\tau_L^2/r_0^2$. For all simulations the particle masses are set to $1m_0$.

Care was taken to ensure that the centre of mass of all particles did not acquire an angular momentum from coupling to the thermostat. This restriction is achieved by subtracting at each step from all particle velocities the vector $\omega_{CM} \times \mathbf{x}_i/N$, with ω_{CM} the angular velocity of the centre of mass, $\mathbf{x}_i$ the position vector of particle i, and N the number of particles. After subtracting this component, the velocities are all rescaled such that the kinetic energy before and after the correction is unchanged. Note, however, that the kinetic energy is not constant, as the Langevin thermostat imposes fluctuations consistent with the canonical ensemble. Because the particles are constrained to the surface of a sphere, there is no need to subtract the linear velocity of the centre of mass.

For both potentials, we attempt to find for all $10 \leq N \leq 100$ the potential energy minimum using the basin-hopping method[31] as well as thermal equilibrium packings in a temperature range between $T = 0.001\varepsilon/k_B$ and $T = 2\varepsilon/k_B$, where k_B is Boltzmann's constant. For each N a surface density ρ has to be chosen. Let R be the radius of the spherical surface. Then $\rho = N/4\pi R^2$, and R has to be determined for each N. A natural choice for R is the radius that results in the lowest potential energy at zero temperature. For Lennard-Jones potentials, these radii are tabulated by Voogd in ref. 13 and are consistent with our basin-hopping calculations, but for a Morse potential we have not been able to find tabulated values. We therefore employ the following strategy.

We perform Langevin dynamics simulations of N particles constrained to a sphere using a special case of the RATTLE algorithm[32] described in ref. 33, where we linearly shrink the radius from an initial value R_0 to a final value R_1 over a time span of $10^4\tau_L$. The values for R_0 and R_1 we estimate from considerations of hard disk packings, which gives rise to a natural sphere radius R^*. To calculate R^*, consider N hard disks of diameter d_0 that cover an area fraction $\phi = Nd_0^2/16R^2$ of the sphere. The upper limit to ϕ in a flat, two-dimensional geometry is $\phi_m = \pi/\sqrt{12}$.[3] The radius that gives this maximum is then $R^* = d_0\sqrt{N/\phi_m}/4$. With d_0 we associate the minimum of the interaction potential r_0, because for $r < r_0$ both potentials are steeply repulsive.

We search for a minimum in the potential energy around R^* by putting $R_0 = 1.3R^*$ and $R_1 = 0.8R^*$. For each N we monitor over time the potential energy and radius of the spherical template as it shrinks from R_1 to R_0. This schedule produces an energy trace for each N as a function of R similar to those presented by Voogd,[13] with a characteristic deep minimum just before a steep increase for small R, from which the optimal radius can be determined with a simple post-processing script.
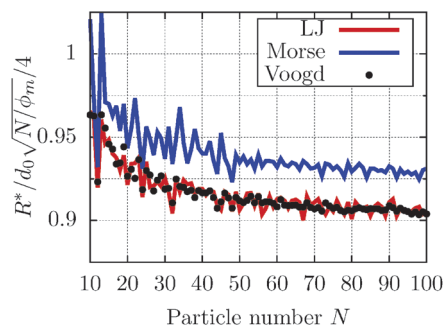
Fig. 1 Sphere radii R^* that minimise the potential energy for N particles interacting either through a Lennard-Jones (LJ) or a Morse (Morse) potential, as fraction of the estimated radius that would tightly pack N hard disks of diameter d_0, $d_0\sqrt{N/\phi_{\mathrm{M}}}/4$. Note that the LJ data coincides well with the results of Voogd (reproduced with permission).[13] The largest difference between the two is no more than $0.02r_0$ ($<2\%$).

We present the optimal radii R as a function of N in Fig. 1 for both the Lennard-Jones and Morse particles for the case $\alpha = 60/r_0$. Note that for the Morse particles, the sphere radius is larger for all $10 \leq N \leq 100$, because the penalty for overlap is much greater and cannot be compensated easily by next-nearest neighbour interactions. For the Lennard-Jones particles, the difference in the optimal radius R between our data and Voogd's is less than 2% for all N and the largest deviation in total energy is below 1%. Additionally, the potential energies we find at the optimal radius match closely with those presented by Zandi *et al.* in ref. 4. Furthermore, if we use the same method of quantifying defects as Voogd,[13] which is based on Voronoi constructions, we find the same distribution of topological charges, reassuring us that we obtain the same structures. For a complete tabulation of our energies and sphere radii, see Section S1 (ESI†).

While Voronoi tesselation, as used by Voogd, is a natural way to determine nearest neighbours in a hexagonal lattice, issues arise with Voronoi tesselation when particles are packed in other types of lattice, as the tesselation can be degenerate. These issues are discussed in more detail in Section S2 (ESI†). In previous works on global energy minima of the Thomson problem such configurations were encountered,[14,17] so this apparent pathology was anticipated in the present work. Because of these problems, we opted instead for a distance criterion to quantify the number and type of defects.

With this criterion, all particles separated by less than a distance r^* are considered nearest neighbours. In this case, care has to be taken to select a sensible value for r^*. One way to do this is to determine for every N at what distance the second minimum in the pair distribution function is located and to use this to fix r^*. Some structures, however, produce a split first peak at around the minimum of the potential energy $r = r_0$. In that case, we choose as r^* a distance after the split peak but before the second major peak.

In principle, r^* is a function of temperature, so it should be determined for every temperature T. For practical reasons, however, we determine r^* only at the low temperature of $T = 0.01\varepsilon/k_{\mathrm{B}}$. For $N = 24, 32, 44, 48$ and 72 we verified that r^* obtained

this way still coincides with a minimum in the time-averaged pair correlation function at a higher temperature of $T = 0.5\varepsilon/k_{\mathrm{B}}$. With the distance criterion, square lattices are identified more robustly in the presence of thermal fluctuations than by means of tesselation, especially at lower temperatures. See Section S3 (ESI†) for a more thorough description of this procedure and a tabulation of the cut-off radii r^* obtained. Note, however, that the network generated by connecting the nearest neighbours in general does not have the proper Euler characteristic, an issue we choose to ignore. Because of the drawbacks associated with both methods, we apply both and compare them.

For the representative case of $N = 72$ particles, we determine the free energy difference between specific packings as a function of temperature to extract the relative contributions of potential energy and entropy. Our first attempts to determine these properties with thermodynamic integration as described in ref. 34 did not produce satisfactory results. However, since in our simulations the packings fluctuate between different symmetries, we count their occurrence frequencies. From these frequencies we can reconstruct at each temperature the probability of finding a packing. From the probability ratio for two different configurations, say, a and b, we calculate a free energy difference. The probability P_a of encountering a scales with the Boltzmann factor as $P_a \sim \exp(-F_a/k_{\mathrm{B}}T)$, where F_a is the free energy of packing a. Hence, the ratio of two of these probabilities is $P_a/P_b = \exp(-(F_a - F_b)/k_{\mathrm{B}}T) = \exp(-\Delta F_{ab}/k_{\mathrm{B}}T)$. In other words, $\Delta F_{ab} = -k_{\mathrm{B}}T\ln(P_a/P_b)$. Entropy differences can be derived from the slope of the free energy difference as a function of temperature, since $S = -(\partial F/\partial T)_{N,R}$ evaluated at constant particle number N and sphere radius R.

We next consider the thermal stability of Lennard-Jones packings in Section 3 by investigating the number of point defects at various temperatures. We then focus in Section 4 on some packings that have additional defects in the global minimum, and we determine their stability at different temperatures by calculating the free energy. Finally we perform the same stability analysis for a short-ranged Morse potential in Section 5.

3 Lennard-Jones defect landscape

For the Lennard-Jones potential we determine the number of point defects as a function of temperature and particle number. Point defects are particles that do not have six nearest neighbours. For completeness and to facilitate straight-forward comparison with earlier work, *e.g.*, ref. 13, we present results using the distance criterion in this section and those with the Voronoi tessellation in Section S2 (ESI†). The data for $T = 0$ are generated by means of basin-hopping calculations with the aid of the GMIN program.[31,35] The data for $T > 0$ are obtained from a Langevin dynamics simulation using the LAMMPS program.[30] The damping time of the thermostat, τ_{L}, is the reference time unit, while the time step size is fixed at $0.005\tau_{\mathrm{L}}$. The time step size was chosen empirically by finding a value for which the particles have good energy conservation properties, when the thermostat is disabled. For the Langevin thermostat we invoked
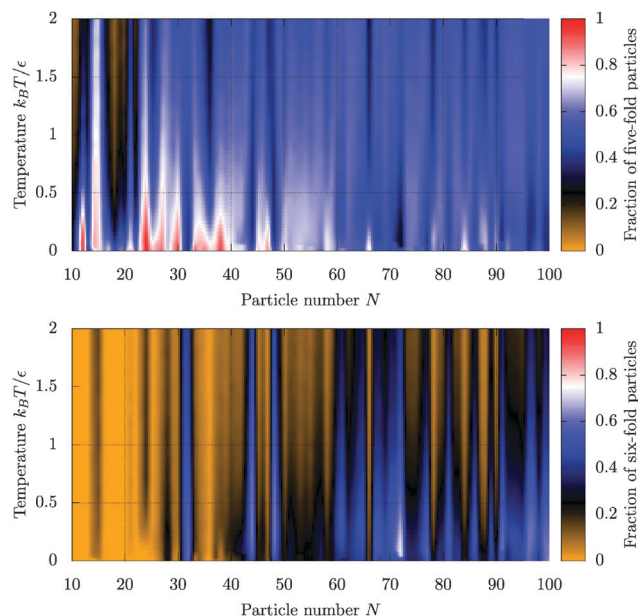
Fig. 2 Fraction of particles with five (top) and six (bottom) neighbours as a function of temperature for $N = 10$ to $N = 100$ Lennard-Jones particles, using the distance criterion. For the (small) fraction of particles with seven neighbours, see Fig. S3 (ESI†). Other numbers of nearest neighbours were not observed.

Fig. 3 The five Lennard-Jones packings for $N = 72$ with the lowest potential energy found using the GMIN program[35] from two different orientations (top and bottom) (a) D_{5h} packing with energy per particle $U/N = -3.0564\varepsilon$, (b) D_3 packing with $U/N = -3.0559\varepsilon$, (c) icosahedral packing with $U/N = -3.0548\varepsilon$, (d) tetrahedral packing with $U/N = -3.04636\varepsilon$ and (e) packing with two times three rectangular patches that wrap around the sphere similar to the seam on a baseball, with $U/N = -3.04630\varepsilon$. The colour indicates the coordination numbers five (blue) or six (red).

Fig. 4 Excess defect fraction for $N = 38$, 44, 48, 60, 72 and 92. Lennard-Jones particles as a function of temperature as determined by the distance criterion. Note the reentrance of excess defects with increasing temperature for $N \neq 24$.

the Grønbech-Jensen–Farago formulation,[36] which generates positions that are correctly Boltzmann distributed at the thermostat temperature for larger time steps, albeit at the expense of inaccuracies in the velocity distribution. Since none of the properties we are interested in depend on the velocity distribution, this is an acceptable drawback.

In Fig. 2 we show the fractions of particles with five and six nearest neighbours within the distance r^* at which the pair distribution function has its second minimum. In Fig. S3 (ESI†) we present the fraction of particles with seven nearest neighbours, which we find to be lower than 0.02 for all N and T. From Fig. 2 we see that for many N there are more than twelve particles with five nearest neighbours across the entire temperature range probed. Apart from $N = 12$, $N = 32$ is the only packing that retains icosahedral symmetry for a large temperature range. For low temperatures it has exactly 12 five-fold particles, for a fraction of $12/32 = 0.375$. If the temperature is increased to $T = 2\varepsilon/k_B$, four more five-fold particles appear, leading to an increased five-fold fraction of $16/32 = 0.5$. This indicates that the $T = 3$ icosahedral structure of 32 particles is very robust against thermal fluctuations, as it exhibits a smaller increase in excess defects than packings with other N.

Typically, the number of excess defects increases with temperature. Remarkably, however, for certain N we observe additional defects in the ground state and a non-monotonic dependence of the number of defects as a function of temperature, most notably for $N = 44$, 48 and 72. $N = 72$ is particularly interesting because one might expect the minimum energy structure to be a $T = 7$ icosahedron. While the icosahedron is a low energy minimum, it turns out there are two more packings with a lower potential energy, namely, a D_{5h} structure and a D_3 structure, as
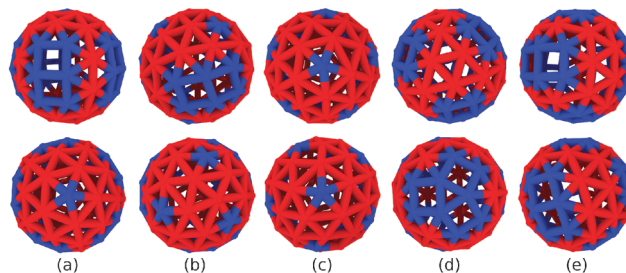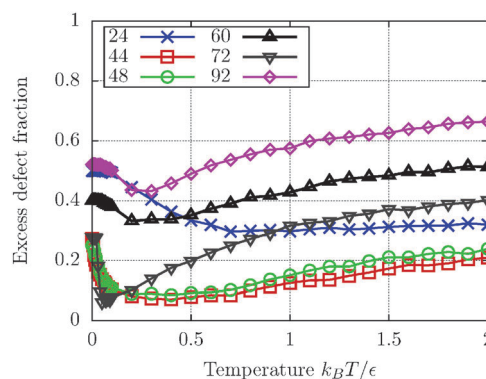
well as two additional packings with a slightly higher potential energy, one of which exhibits tetrahedral symmetry. We present all of them in Fig. 3. Apart from the icosahedral structure in Fig. 3c, they all exhibit clusters of point defects. The two lowest minima have square arrangements of particles. From this result we can conclude that for $N = 72$ an icosahedral packing is stabilised entropically rather than energetically. We demonstrate that this is indeed the case in Section 4. Note that there are other N values for which excess defects disappear at intermediate temperatures, e.g., $N = 24$, 44, 48, 60 and 90. For all these sizes but $N = 24$, excess defects reappear at higher temperatures. The excess defect fraction for these N values is plotted as function of temperature in Fig. 4.

4 Defects near the ground state

As we have seen in Section 3, some values of N produce packings that exhibit excess defects at very low temperatures. For two thirds of the clusters considered, the number of excess defects obtained for $T = 0$ by means of basin-hopping is equal to the number of excess defects at the lowest non-zero temperature

result from our Langevin dynamics simulation ($T = 0.001\varepsilon/k_B$). This correspondence suggests that these packings are not the result of kinetic trapping but are energetically stabilised. Some sizes, however, exhibit a discrepancy between the two approaches.

The even N for which there was a minor discrepancy in the excess defect fraction between these two simulations were $N = 28, 30, 50, 58, 74, 94,$ and 98. For these packings, the particles fluctuate between different low energy structures even at this low temperature, and therefore the average number of excess defects does not exactly match the number of excess defects in the global minimum. The largest relative deviation in the excess defect fraction between the two is 0.14% for $N = 30$. From this result we conclude that if we would go to even lower temperatures, we would get the right structures because the global minimum dominates. We have not pursued this limit further on account of the very long equilibration times required for proper sampling.

For the odd particle numbers, we see similar discrepancies, namely for particle numbers $N = 37, 39, 41, 43, 47, 51, 55, 59, 73, 79, 85$ and all odd $N \geq 89$, where the largest discrepancy in the excess defect fraction amounts to 0.12%. Again, at the lowest non-zero temperature tested, the particle packing fluctuates between different symmetries, where the dominant structure is the global minimum. For all other odd and even N, we found no discrepancies between the two methods.

For some N that exhibit excess defects in the low temperature regime, we find that these defects disappear at intermediate temperatures and reappear at higher temperatures. This effect occurs for even $N = 28, 40, 42, 46, 60, 62, 64, 68, 72, 76$ and 86, and for odd $N = 37, 39, 41, 61, 71, 91$ and 97. To investigate this unexpected behaviour we focus attention on $N = 72$, for which we know that the lowest temperature Langevin dynamics packing coincides with the zero temperature basin-hopping result. Apart from the global minimum, basin-hopping finds four additional local potential energy minima with a significantly lower potential energy than the other local minima (1.4% difference). The differences in potential energy between the five lowest energy packings are very small ($<0.04\%$). Recall that these minimum energy structures are shown in Fig. 3.

In order of increasing potential energy, the symmetries of these packings are D_{5h}, D_3, icosahedral, tetrahedral, and finally a packing consisting of two domains containing three rectangular patches that wrap around each other, similar to a baseball pattern. Of these five packings, only those that correspond to the lowest three potential energy minima, (a), (b) and (c) in Fig. 3, are observed in our LD simulations at low but non-zero temperatures, indicating that either the barrier between these three states and the other two is too large, or that the free energy difference destabilises the two packings with higher potential energy. Taking into account the contribution of the potential energy to the Boltzmann weight of a configuration, in particular near zero temperature, this last explanation seems plausible. For these low potential energy packings we present the ratios of the calculated Boltzmann factors for six temperatures in Table 1. We calculated these Boltzmann factors from the potential energies of the packings obtained by means of

Table 1 Estimated relative probabilities of observing a D_3 (Fig. 3b), icosahedral (ico, Fig. 3c), tetrahedral (tetra, Fig. 3d) or a packing with two domains with three rectangular patches (rect, Fig. 3e) compared to that of finding D_{5h} (Fig. 3a), using the Boltzmann weight of the respective calculated potential energy

$k_B T/\varepsilon$	0.001	0.01	0.02	0.03	0.04	0.05
$P(D_3)/P(D_{5h})$	0.556	0.943	0.971	0.980	0.985	0.988
$P(\text{ico})/P(D_{5h})$	0.199	0.851	0.922	0.948	0.960	0.968
$P(\text{tetra})/P(D_{5h})$	4.18×10^{-5}	0.365	0.604	0.715	0.777	0.817
$P(\text{rect})/P(D_{5h})$	3.95×10^{-5}	0.363	0.602	0.713	0.776	0.816

basin-hopping, given in the caption to Fig. 3. From Table 1 it is clear that at very low temperatures the potential energy differences are amplified and that this is what destabilises the tetrahedral and baseball packings.

To quantify the free energy rather than the potential energy differences between the three packings found in our dynamics simulations, we determine the frequency of occurrence of the different packings, as outlined in Section 2. To verify ergodicity, we keep track of the normalised frequencies of each packing as a function of time, and verify that they reach a steady state value. We also keep track of how often the packings switch between the identified types. For a detailed analysis, see Section S5 (ESI†). In particular, in Fig. S7 (ESI†) we show two time traces of the observed packings and in Fig. S8 (ESI†) we show the convergence of the observed frequencies. For $T > 0.03\varepsilon/k_B$ we are close to achieving steady states, and we presume ergodicity to hold for those temperatures.

In Fig. 5 we show the frequencies at which the different packings occur as a function of temperature. Note that at low temperatures, the low potential energy packings D_3 and D_{5h} are energetically stabilised, while the icosahedral packing is completely suppressed. At higher temperatures, the icosahedral packing becomes more and more dominant, while the D_{5h} and D_3 packings become entropically suppressed. Basin-hopping predicts a D_{5h} packing for the global potential energy minimum, which is consistent with the trend shown in Fig. 5, but reliable
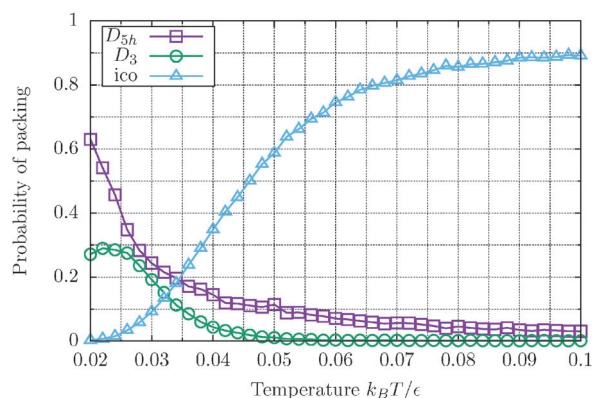
Fig. 5 Probability of encountering an icosahedral, D_{5h} or D_3 packing with $N = 72$ Lennard-Jones particles on a sphere with radius $R = 2.55037r_0$, where r_0 is the equilibrium spacing of the pair potential, as a function of the dimensionless temperature $k_B T/\varepsilon$. The frequencies do not sum to unity because for some time frames the packing could not be identified.
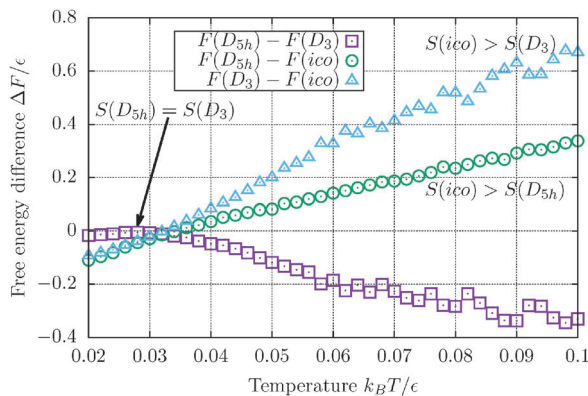
Fig. 6 Free energy differences between packings of $N = 72$ particles on a sphere radius $R = 2.55037r_0$. At low temperatures the D_3 and D_{5h} packings are nearly equal in free energy, but an increasing importance of entropy destabilises the D_3 packing more than the D_{5h} at higher T. Both the D_{5h} and D_3 packing are destabilised at higher k_BT in favour of the icosahedral packing. At $k_BT \approx 0.032\varepsilon$ the three packings appear to be equally probable.

data for the temperatures in between $T = 0$ and $0.03\varepsilon/k_B$ are difficult to obtain due to the increased simulation time needed for proper sampling. Thus, while for $T \leq 0.03\varepsilon/k_B$ the trend seems to be consistent with the basin-hopping calculations, the exact values for the frequencies might not be as reliable. For $T > 0.03\varepsilon/k_B$ a clear steady state was reached that converged for all three initial packings, and we presume these data to be reliable.

Using the relative occurrence frequencies of the different symmetries we extract free energy differences, presuming ergodicity, from the associated Boltzmann weights. In Fig. 6 we plot these free energy differences, from which we immediately see that at around $T \approx 0.032\varepsilon/k_B$ all three packings are equally likely, and that above this temperature the free energy of an icosahedral packing is the lowest. Thus, above $T = 0.032\varepsilon/k_B$, we expect to see predominantly the icosahedral packing, which is consistent with Fig. 5.

We can determine entropy differences by calculating the slope of ΔF, since $S = -(\partial F/\partial T)_{N,R}$, evaluated at constant particle number N and spherical template radius R. This analysis immediately reveals that the entropy of an icosahedral packing is larger than that of both the D_{5h} and D_3 packings, as the slopes of $F(D_{5h})$–F(ico) and $F(D_3)$–F(ico) are positive for the entire temperature range probed. Also note that the entropy of the D_{5h} packing is larger than that of the D_3 packing for most temperatures, as $F(D_{5h})$–$F(D_3)$ has a negative slope for $T > 0.025\varepsilon/k_B$. Hence, at higher temperatures, the icosahedral packing is favoured over both the D_{5h} and D_3 packings due to its higher entropy, while at low temperatures the D_{5h} packing is preferred due to its low potential energy and the fact that its entropy is higher than that of the D_3 packing.

For even larger temperatures $T > 0.1\varepsilon/k_B$ the icosahedral packing becomes less stable because of the emergence of thermally excited excess defects, as is clear from Fig. 2. For this range of temperatures we did not explicitly obtain a free energy difference because we find many different packings, none of which seem to be

clear potential energy minima. These results confirm, not surprisingly, that the equilibrium packings of particles on a curved surface are not just a result of potential energy minimisation but rather of free energy minimisation. Finally, it is clear that on curved surfaces, additional point defects can actually lower the potential energy, and are thus energetically stabilised. Although we have only explicitly shown this for $N = 72$, we hypothesise that the same effect occurs for other particle numbers that exhibit additional defects in the ground state, which disappear for intermediate temperatures, *e.g.*, $N = 60$ and $N = 92$.

Now that we have shown that the temperature, or, equivalently, the interaction strength, plays a crucial role in stabilising different packings, we turn to the role of the range of attraction of the interaction potential.

5 Morse defect landscape

In the previous section we saw that for Lennard-Jones particles there exist energetically stabilised defects at low temperatures. Furthermore, we found that icosahedral packings are stabilised energetically for $N = 32$ but only entropically for $N = 72$. Since a shorter ranged potential is a more realistic model in the context of colloidosomes and virus capsomeres, it is of interest to see how robust our findings are if we reduce the effective range of the interaction potential. We set the range parameter $\alpha = 60/r_0$, as discussed in Section 2, and again determined the excess point defect landscape as a function of particle number N and temperature T. Since this larger value of the parameter α makes the potential sharper around the minimum, a smaller time step is needed to maintain stability. Following the same procedure described in Section 3, we found a time step size of $\Delta t = 5 \times 10^{-4}\tau_L$ to be adequate.

In Fig. 7 we show the number of particles with 5 and 6 nearest neighbours obtained by the distance criterion. In Fig. S4–S6 (ESI†) we also show the fraction of particles with three–four and seven nearest neighbours. Particles with seven nearest neighbours are very rare, with the highest fraction being 0.001 for $T \approx 1.8\varepsilon/k_B$ and $N = 86$. Three and four nearest neighbours occur more frequently for smaller N than compared to the Lennard-Jones packings, which can also be seen from the optimal template radii in SI 1 (ESI†). Note that for the Morse potential, $N = 32$ has no additional defects in the ground state, indicating that the icosahedral packing is again energetically stabilised. The fraction of particles with five nearest neighbours is 0.375, independent of the temperature. For $N = 72$, however, there is no longer an intermediate temperature range for which the icosahedral packing is thermally stabilised.

The ground state of the $N = 72$ packing obtained by basin-hopping consists of three strips of particles with six-fold coordination surrounded by those with five-fold coordination (see Fig. 8a). The packing corresponding to the second-lowest local potential energy minimum is shown in Fig. 8b, where the potential energy is 0.068% larger. The other local potential energy minima have significantly higher energies, with the third-lowest having a potential energy 3.4% larger than the second-lowest.
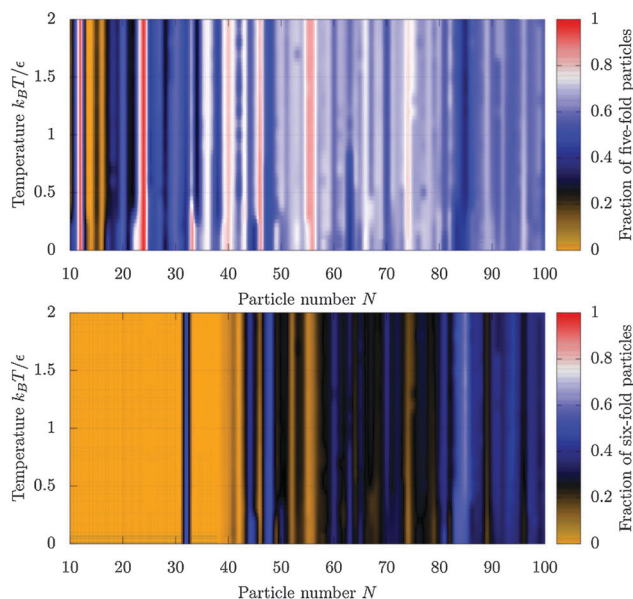
Fig. 7 Fraction of particles with five (top) and six (bottom) neighbours as a function of temperature for $N = 10$ to $N = 100$ Morse particles with $\alpha = 60/r_0$, using the distance criterion. For the fraction of particles with three, four and seven neighbours, see Section S4 (ESI†). Other numbers of nearest neighbours were not observed.
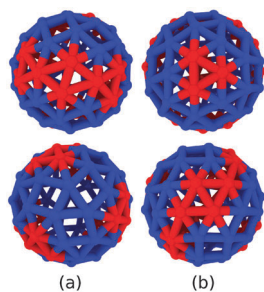
Fig. 8 The two lowest potential energy packings for $N = 72$ particles for a Morse potential with effective range parameter $\alpha = 60/r_0$, where r_0 is the pair potential equilibrium spacing, shown from two sides (top and bottom). Colour codes the number of nearest neighbours (using the distance criterion) of 5 (blue) or 6 (red). (a) The packing with the lowest observed potential energy $U/N = -2.32506\varepsilon$. (b) The second lowest local potential energy minimum with $U/N = -2.32348\varepsilon$.

In our Langevin dynamics simulations the two packings shown in Fig. 8 are also the most dominant ones. Even at $T = 2\varepsilon/k_B$ the system tends to fluctuate between these two packings, where the second minimum shown in Fig. 8b only appears very infrequently. See Fig. S7 (ESI†) for more analysis on the fluctuations between the different packings. Therefore, it seems that for shorter-ranged potentials the energetic penalty is more difficult to overcome by entropy.

From these findings, it seems that a shorter-ranged potential destabilises icosahedral symmetry as expected.[3,28,29] For virus capsids this result would imply that, if the capsomeres are all one size, their effective range parameter should be smaller than $\alpha < 60/r_0$. On the other hand, icosahedral packings can be made more stable by switching between different particle sizes, as
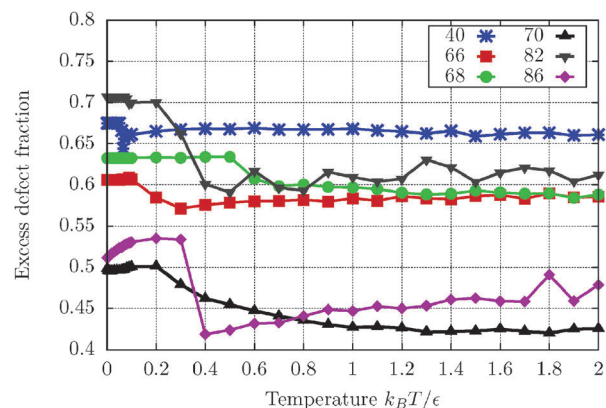
Fig. 9 Temperature dependence of the fraction of excess defects for $N = 40$, 66, 68, 70, 82, 86 and 90 Morse particles with range parameter $\alpha = 60/r_0$.

discussed by Bruinsma, Zandi et al.[3,4] We intend to pursue this question in future work.

Our simulations highlight two major differences between the Lennard-Jones and Morse particle packings. First, we note that excess defects are barely excited at higher temperatures for particles interacting via the short-ranged Morse potential. This is not entirely surprising because the Morse potential considered here is much steeper than the Lennard-Jones potential, implying that at equivalent thermal energies Morse particles have less opportunity to rearrange. Second, and perhaps more strikingly, clusters with $N > 32$ that exhibit a local minimum in the potential energy for both potentials correspond to very different arrangements. These features result in different numbers of excess defects for the two potentials for the same N and T. This analysis confirms that the range of the potential is very important for determining which particle arrangement is the most favourable.[28,29]

For some N, Morse particles exhibit additional defects in the ground state that are energetically stabilised. This result is true for $N = 40$, 66, 68, 70, 82, 86 and 90 although for Morse particles the effect is less pronounced, i.e., the range of variation in the excess defect fraction is not as large as for the Lennard-Jones particles. In fact, the range of variation is so small that it is almost indiscernible in Fig. 7. Hence, we also plot the excess defect fraction as a function of temperature for the N values quoted in Fig. 9. From the figure, we conclude that these sizes show a clear non-monotonic behaviour in the excess defect fraction with increasing temperature, indicating that the defects at low T for these packings are energetically stabilised, just like the defects we find for the Lennard-Jones packings in Fig. 2.

6 Conclusions

Inspired by virus capsid and colloidosome assemblies, we have studied by means of computer simulation the packings from $N = 10$ to 100 point particles constrained to a spherical surface. Our aim was to investigate how the optimal particle arrangements are influenced by temperature, or, equivalently, interaction strength, and the range of the interaction potential. These factors have not received extensive attention in the literature, although we find

from our simulations that both have a profound impact. The simulation techniques that we applied involved Langevin dynamics for non-zero temperatures and basin-hopping calculations for determining the global potential energy minima, which confirm that our Langevin simulations are not kinetically trapped at low temperatures. We have focused mainly on how the number and configuration of point defects, as a measure for the structural stability of packings, vary with temperature. Since at least twelve five-fold point defects are required by geometry, we focus specifically on the number of defects in excess of these twelve.

For N = 12, 32 and 72 Lennard-Jones particles, we find in the temperature range of $T = 0.05\varepsilon/k_B$ to $T = 0.067\varepsilon/k_B$ that the equilibrium packing is an icosahedron, consistent with the earlier work of Zandi et al.[4] Our basin-hopping calculations show that the icosahedral packing is the global potential energy minimum for N = 12 and 32, but not for 72, for which the global minimum is a D_{5h} packing, in agreement with the results of Voogd.[13] This result is surprising because the D_{5h} packing exhibits additional defects, which apparently have an energetically stabilising effect. Hence, the icosahedral structure for N = 72 at non-zero temperature must be entropically stabilised. In fact, our simulations suggest that for a fairly large number of particle packings the lowest energy structure exhibits excess defects that, remarkably, disappear when raising the temperature. Of course, at higher temperatures still, defects become thermally excited. For these specific particle numbers the number of defects is a non-monotonic function of temperature, whilst for all others, the number of defects increases with temperature monotonically.

To investigate this kind of "reentrant" behaviour in more detail, we consider N = 72 Lennard-Jones particles, for which we have explicitly determined free energy differences between the three lowest-energy structures. We find that packings with more excess defects have a lower free energy at sufficiently low temperatures, implying that they are energetically favoured over packings with fewer defects. The global potential energy minimum has D_{5h} symmetry. However, our calculations show that the T = 7 icosahedral packing has a higher entropy than the D_{5h} packing and is therefore thermally stabilised at higher but not too high temperatures. Therefore the packing of Lennard-Jones particles on curved surfaces is not just governed by minimisation of the potential energy. What is true for N = 72 seems to be true for many sizes, because the symmetries of the associated packings exhibit a strong temperature dependence. On the other hand, the T = 3 icosahedral symmetry for N = 32 particles is stable over a wide temperature range.

Our main conclusions are not significantly altered if we replace the Lennard-Jones potential by a short-ranged Morse potential, which arguably is more representative of attractive interactions between large molecules or colloidal particles, because it accounts for a larger excluded volume effect.[24,28] Again we find that for certain sizes, the number of excess defects is a non-monotonic function of the temperature s although for most packings we find that it is more difficult to thermally excite additional defects. The latter result implies that packings of particles with a shorter range of attraction are more stable against thermal fluctuations. Another notable difference between Lennard-Jones and Morse particles is that for equal N and T, the equilibrium packings may exhibit different symmetries. In particular, this is the case for N > 24, with the exception of the T = 3 icosahedron for N = 32. Unfortunately, for a shorter-ranged Morse potential, rearrangements of packings become too rare to determine entropies of packings through simply counting their frequencies. A dedicated free energy method like free energy basin-hopping might provide more insight for these types of potentials.[37]

Our calculations suggest that equilibrium particle geometries on a curved surface depend not only on the strength but also on the exact shape of the interaction potential. Both factors impact upon to what extent temperature is able to affect the competition between particle packings.

Acknowledgements

References

1 D. L. D. Caspar and A. Klug, *Cold Spring Harbor Symp. Quant. Biol.*, 1962, **27**, 1–24.
2 A. D. Dinsmore, M. F. Hsu, M. G. Nikolaides, M. Marquez, A. R. Bausch and D. A. Weitz, *Science*, 2002, **298**, 1006–1009.
3 R. F. Bruinsma, W. M. Gelbart, D. Reguera, J. Rudnick and R. Zandi, *Phys. Rev. Lett.*, 2003, **90**, 248101.
4 R. Zandi, D. Reguera, R. F. Bruinsma, W. M. Gelbart and J. Rudnick, *Proc. Natl. Acad. Sci. U. S. A.*, 2004, **101**, 15556–15560.
5 R. Fantoni, J. W. O. Salari and B. Klumperman, *Phys. Rev. E: Stat., Nonlinear, Soft Matter Phys.*, 2012, **85**, 061404.
6 R. Backofen, A. Voigt and T. Witkowski, *Phys. Rev. E: Stat., Nonlinear, Soft Matter Phys.*, 2010, **81**, 025701.
7 M. J. W. Dodgson and M. A. Moore, *Phys. Rev. B: Condens. Matter Mater. Phys.*, 1997, **55**, 3816–3831.
8 A. Pérez-Garrido and M. A. Moore, *Phys. Rev. B: Condens. Matter Mater. Phys.*, 1999, **60**, 15628–15631.
9 M. J. Bowick, D. R. Nelson and A. Travesset, *Phys. Rev. B: Condens. Matter Mater. Phys.*, 2000, **62**, 8738–8751.
10 A. R. Bausch, M. J. Bowick, A. Cacciuto, A. D. Dinsmore, M. F. Hsu, D. R. Nelson, M. G. Nikolaides, A. Travesset and D. A. Weitz, *Science*, 2003, **299**, 1716–1718.
11 M. J. Bowick, A. Cacciuto, D. R. Nelson and A. Travesset, *Phys. Rev. B: Condens. Matter Mater. Phys.*, 2006, **73**, 024115.
12 H. Kusumaatmaja and D. J. Wales, *Phys. Rev. Lett.*, 2013, **110**, 165502.
13 J. M. Voogd, PhD thesis, Universiteit van Amsterdam, 1998.
14 D. J. Wales and S. Ulker, *Phys. Rev. B: Condens. Matter Mater. Phys.*, 2006, **74**, 212101.
15 S. N. Fejer, D. Chakrabarti and D. J. Wales, *ACS Nano*, 2010, **4**, 219–228.
16 E. L. Altschuler and A. Pérez-Garrido, arXiv, 2009.
17 D. J. Wales, H. McKay and E. L. Altschuler, *Phys. Rev. B: Condens. Matter Mater. Phys.*, 2009, **79**, 224115.

18 K. J. Strandburg, *Rev. Mod. Phys.*, 1988, **60**, 161–207.

19 A. Lomakin, N. Asherie and G. B. Benedek, *Proc. Natl. Acad. Sci. U. S. A.*, 2003, **100**, 10254–10257.

20 W. K. Kegel and P. van der Schoot, *Biophys. J.*, 2004, **86**, 3905–3913.

21 P. Prinsen and T. Odijk, *J. Chem. Phys.*, 2006, **125**, 074903.

22 V. A. Parsegian, *Van der Waals Forces*, Cambridge University Press, Cambridge, 2005.

23 G. Meng, J. Paulose, D. R. Nelson and V. N. Manoharan, *Science*, 2014, **343**, 634–637.

24 J. P. K. Doye, D. J. Wales and R. S. Berry, *J. Chem. Phys.*, 1995, **103**, 4234–4249.

25 D. J. Wales, *ChemPhysChem*, 2010, **11**, 2491–2494.

26 C. J. Burke, B. L. Mbanga, Z. Wei, P. T. Spicer and T. J. Atherton, *Soft Matter*, 2015, **11**, 5872–5882.

27 M. H. J. Hagen, E. J. Meijer, G. C. A. M. Mooij, D. Frenkel and H. N. W. Lekkerkerker, *Nature*, 1993, **365**, 425–426.

28 J. P. K. Doye and D. J. Wales, *J. Phys. B: At., Mol. Opt. Phys.*, 1996, **29**, 4859.

29 J. P. K. Doye and D. J. Wales, *Science*, 1996, **271**, 484–487.

30 S. Plimpton, *J. Comput. Phys.*, 1995, **117**, 1–19.

31 D. J. Wales and J. P. K. Doye, *J. Phys. Chem. A*, 1997, **101**, 5111–5116.

32 H. C. Andersen, *J. Comput. Phys.*, 1983, **52**, 24–34.

33 S. Paquay and R. Kusters, *Biophys. J.*, 2016, **110**, 1226–1233.

34 *Understanding Molecular Simulation*, ed. D. Frenkel and B. Smit, Academic Press, San Diego, 2nd edn, 2002, pp. xiii–xiv.

35 D. J. Wales, GMIN, http://www-wales.ch.cam.ac.uk/GMIN/, Downloaded on August 20th, 2015 from http://www-wales.ch.cam.ac.uk/GMIN/.

36 N. Grønbech-Jensen and O. Farago, *Mol. Phys.*, 2013, **111**, 983–991.

37 K. Sutherland-Cash, D. Wales and D. Chakrabarti, *Chem. Phys. Lett.*, 2015, **625**, 1–4.